Langmuir

Article

pubs.acs.org/Langmuir

Partially Crystalline Zn_2GeO_4 Nanorod/Graphene Composites as Anode Materials for High Performance Lithium Ion Batteries

Rui Wang,[†] Songping Wu,*[,†,‡] Yichao Lv,[†] and Zhiqun Lin*[,‡]

[†]School of Chemistry and Chemical Engineering, South China University of Technology, Guangzhou 510641, China

[‡]School of Materials Science and Engineering, Georgia Institute of Technology, Atlanta, Georgia 30332, United States

Supporting Information

ABSTRACT: Zn_2GeO_4 nanorod/graphene composites (ZGCs) were yielded by a two-step hydrothermal processing. Crystalline and amorphous regions were found to coexist in a single Zn_2GeO_4 nanorod. The surface of the Zn_2GeO_4 nanorod was compactly covered and anchored by graphene sheets. The ZGCs were then utilized as anodes for lithium ion batteries (LIBs). Intriguingly, partially crystalline ZGC containing 10.2 wt % graphene possessed excellent electrochemical performance, namely, high reversible capacity (1020 mA h g^{-1} in the first cycle), favorable cyclic performance (768 mA h g^{-1} after 50 cycles), and commendable rate capability (780 mA h g^{-1} at the current density of 0.8A g^{-1}). The amorphous region in partially crystalline Zn_2GeO_4 nanorods and the elastic graphene sheets provided the accommodation of volume change during the charge and discharge processes. These advantageous attributes make ZGCs the potential anode materials for LIBs.

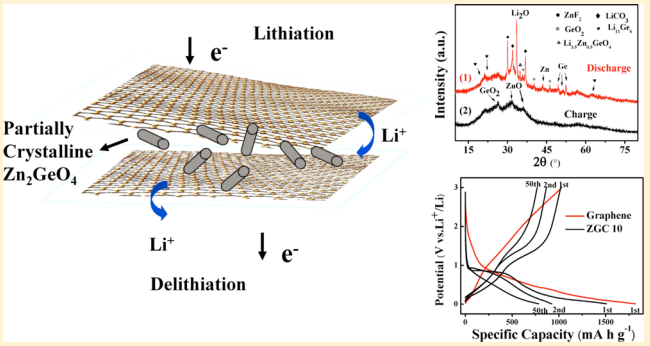

INTRODUCTION

Because of their high energy density and capacity of storing and supplying electricity over a long period of time, lithium-ion batteries (LIBs) have received much attention.[1−3] The commonly used carbon anode materials, specifically graphite, have a low theoretical capacity (~370 mA h g^{-1}). In this context, it is critical to explore new anode materials to improve the capacity of LIBs. The binary and ternary compounds (i.e, GeO_2, Zn_2MO_4 (M = Ge, Sn)) have been used to restrain the volume expansion, improve the capacity, and reduce the costs of LIBs.[4,5] It has been demonstrated that the anodes containing *pure crystalline* Zn_2GeO_4 nanorods prepared by the hydrothermal reaction exhibited a capacity of 616 mA h g^{-1} after 100 cycles.[3] Conversely, pristine rod-like nanocrystalline Zn_2GeO_4 anodes with a capacity below 290 mA h g^{-1} after only 10 cycles were also reported.[6] Quite interestingly, *amorphous* Zn_2GeO_4 nanoparticles were found to be good anode materials for LIBs as well owing to a high reversible specific capacity of 1250 mA h g^{-1}.[7] The amorphous Zn_2GeO_4 was believed to reduce the anisotropic expansion and eliminate the stress during the charge and discharge processes. Clearly, it remains a challenge to rationally design and synthesize Zn_2GeO_4-based nanomaterials with specific microstructures to accommodate the volume expansion in LIBs.

Because of their structural anisotropy, nanorods have garnered significant attention for use in LIBs to decrease the lithium ion diffusion distance and increase the electronic pathway as well as interfacial contact area with electrolytes.[8−10] To this end, ternary oxides with the nanorod-like structures have been regarded as the promising candidate for anode materials in LIBs.[3] Despite the previous work on crystalline Zn_2GeO_4 nanorods[3,6,11] and amorphous Zn_2GeO_4 nanoparticles,[7] mesoporous oxides containing nanocrystalline domains within relatively thick amorphous walls,[12] Zn_2GeO_4 nanorods possessing intriguing partially crystalline structures *have not yet* been reported. On the other hand, two-dimensional graphene is often chosen as the matrix to provide the support for inorganic anode materials[13] due primarily to its large surface area[14] and outstanding conductivity.[15,16] Herein, we report a viable two-step hydrothermal route to partially crystalline Zn_2GeO_4 nanorods/graphene composites (ZGCs) as anodes for high-performance LIBs. The resulting partially crystalline Zn_2GeO_4 nanorods (i.e., containing both crystalline and amorphous regions in a single nanorod) combine the advantages of both amorphous (i.e., the absence of phase change) and crystalline (i.e., well-define crystalline system and rod-like morphology) Zn_2GeO_4. In ZGCs, the graphene sheets and partially crystalline Zn_2GeO_4 nanorods act as the spacers for one another. More importantly, the amorphous region of Zn_2GeO_4 and the elastic graphene sheets offer the collective accommodation for the volume change of partially crystalline Zn_2GeO_4 nanorods during the charge and discharge processes, resulting in an excellent cycling performance. Notably, the partially crystalline ZGC comprising 10.2 wt % graphene

Received: May 12, 2014
Revised: June 17, 2014
Published: June 17, 2014

   dx.doi.org/10.1021/la501830r | *Langmuir* 2014, 30, 8215−8220

exhibited an excellent electrochemical performance, that is, high reversible capacity of 1020 mA h g^{-1} in the first cycle, outstanding cyclic performance of 768 mA h g^{-1} after 50 cycles, nearly 100% Coulombic efficiency, and commendable rate capability of 780 mA h g^{-1} at the current density of 0.8A g^{-1}.

EXPERIMENTAL SECTION

Pure Zn_2GeO_4 nanorods were synthesized using a low-temperature hydrothermal reaction as reported in our previous work.[11] Graphite oxide was prepared with a modified Hummer's method.[17] After being sonicated for 2 h, graphene oxide was added into the solution containing as-synthesized Zn_2GeO_4 nanorods. Subsequently, a second hydrothermal process was conducted. The final product was freeze-dried. Submicron-sized Zn_2GeO_4 particles were synthesized by the solid-state method. Mechanically mixed submicron-sized Zn_2GeO_4 particle/graphite composites were also prepared for comparison. The CR2032-type coin cells were fabricated in a glovebox. The electrochemical performances of active materials were evaluated. More experimental details are described in the Supporting Information.

RESULTS AND DISCUSSION

Figure 1a depicts the XRD patterns of Zn_2GeO_4 nanorod/graphene composites (ZGCs) containing 10.2 wt % graphene (denoted ZGC10; curve 1; see Supporting Information and Figure S1a) and pure Zn_2GeO_4 (curve 2). The emergence of characteristic diffraction peaks is in good agreement with the rhombohedral phase of Zn_2GeO_4 (JCPDS No. 11-0687). The disappearance of the characteristic (002) peak of graphene at $2\theta = 25°$ can be ascribed to the poor crystallization and the absence of considerable layer-to-layer stacking of graphene.[18,19] We note that the XRD results were further substantiated by the XPS (Supporting Information and Figure S2) and Raman measurements (Supporting Information and Figure S3). Taken together, the as-synthesized composites were composed of graphene and Zn_2GeO_4.

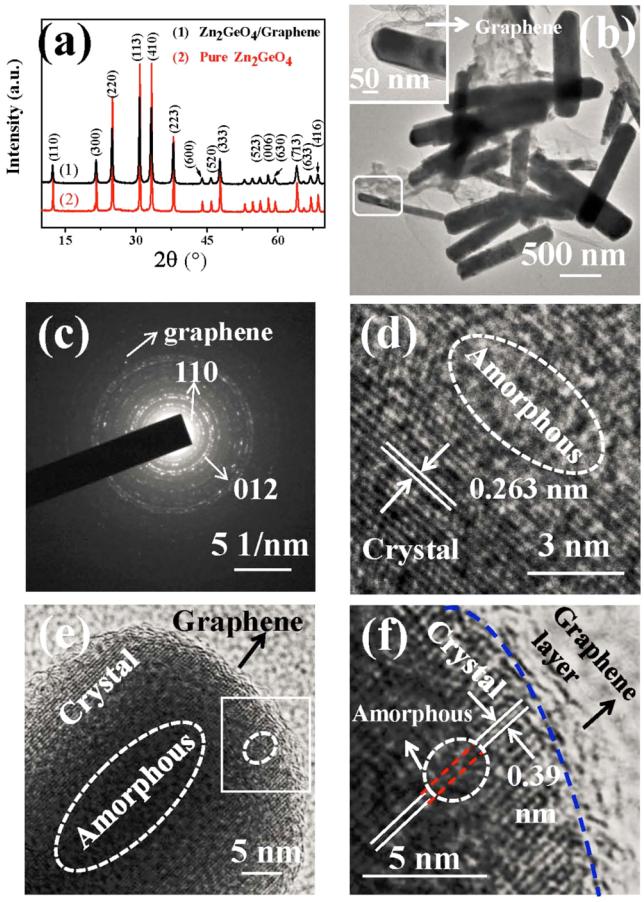

Figure 1. (a) XRD patterns of as-synthesized Zn_2GeO_4/graphene composite (ZGC10) and pure Zn_2GeO_4. (b) TEM images of partially crystalline ZGC10. The close-up of the lower left white-box region in (b) is shown as the inset. (c) SAED pattern of partially crystalline ZGC10. (d, e) HRTEM images of partially crystalline ZGC10 and ZGC9, respectively. (f) Close-up of the central right white-box region in (e).

A representative TEM image of ZGC10 showed that Zn_2GeO_4 nanorods were 1.25 μm long with a diameter of 200 nm (Figure 1b). Of particular interest is that Zn_2GeO_4 nanorods were tightly covered and anchored by highly flexible graphene sheets (inset in Figure 1b, Figure S4b,c and Figure S1b). Furthermore, the selected area electron diffraction (SAED) of ZGC10 containing 10.2 wt % graphene (Figure 1c) displayed two sets of diffraction patterns: one with isolated and disordered dots that were assigned to graphene sheets and the other with ordered rings originating from Zn_2GeO_4 nanorods. Surprisingly, partially crystalline Zn_2GeO_4 nanorods were generally found in ZGCs (e.g., both ZGC10 (Figure 1d) and ZGC9 (Figure 1e), in which both crystalline and amorphous regions coexist in a single Zn_2GeO_4 nanorod). The HRTEM images clearly suggested that the crystalline region of partially crystalline Zn_2GeO_4 nanorods was separated by the amorphous region, at least on the surface of nanorods (Figure 1d–f). The crystalline regions had the lattice spacing of 0.263 nm (Figure 1d) or 0.39 nm (Figure 1f), corresponding to the (410) or (113) lattice plane of the rhombohedral phase of Zn_2GeO_4, respectively. The uniform lattice fringe, the spot-like pattern of SAED, and the corresponding fast Fourier transform (FFT) pattern (inset in Figure S4d) of Zn_2GeO_4 nanorods suggested that each crystalline region was composed of a single crystalline domain. Most importantly, the graphene layer, approximately 2 nm thick, can be clearly observed (Figure 1f), further confirming the formation of graphene sheet-covered Zn_2GeO_4 nanorods. For comparison, the XRD pattern and TEM images of submicron-sized Zn_2GeO_4 particles synthesized by solid-state method are shown in Figure S5.

The electrochemical impedance spectroscopy (EIS) measurements on graphene, ZGC10 and ZGC9 were performed to study the effect of the addition of graphene on conductivity after the 1st cycle (Figure 2a). Obviously, the resistance originating from the surface film and charge transfer (i.e., $R(sf + ct)$)[20] increased with the increased amount of graphene, from 28 Ω for graphene to 168 Ω for ZGC9, based on the equivalent electrical circuit model analysis (Figure S6).[20] The largely improved conductivity of ZGC10 (i.e., $R(sf + ct) = 132$ Ω as compared to 168 Ω for ZGC9) provided the tangible contribution to electrochemical performance in LIBs. The charge/discharge cycling at the constant current was performed to evaluate the electrochemical performance of partially crystalline ZGCs as electrode materials for LIBs. The pure Zn_2GeO_4 nanorods (approximately 100–150 nm in length and 50 nm in diameter, Figure S4a), pure graphene, and Zn_2GeO_4/graphite composites (under 50 mA g^{-1}) were also employed as controls to highlight the advantages of partially crystalline ZGCs as electrode materials. Figure 2b compares the charge/discharge of graphene and composite electrodes at the 1st cycle and the 1st, 2nd, and 50th cycles at a current density of 200 mA h g^{-1}, respectively. For the ZGC10 and Zn_2GeO_4/grphite

dx.doi.org/10.1021/la501830r | Langmuir 2014, 30, 8215–8220

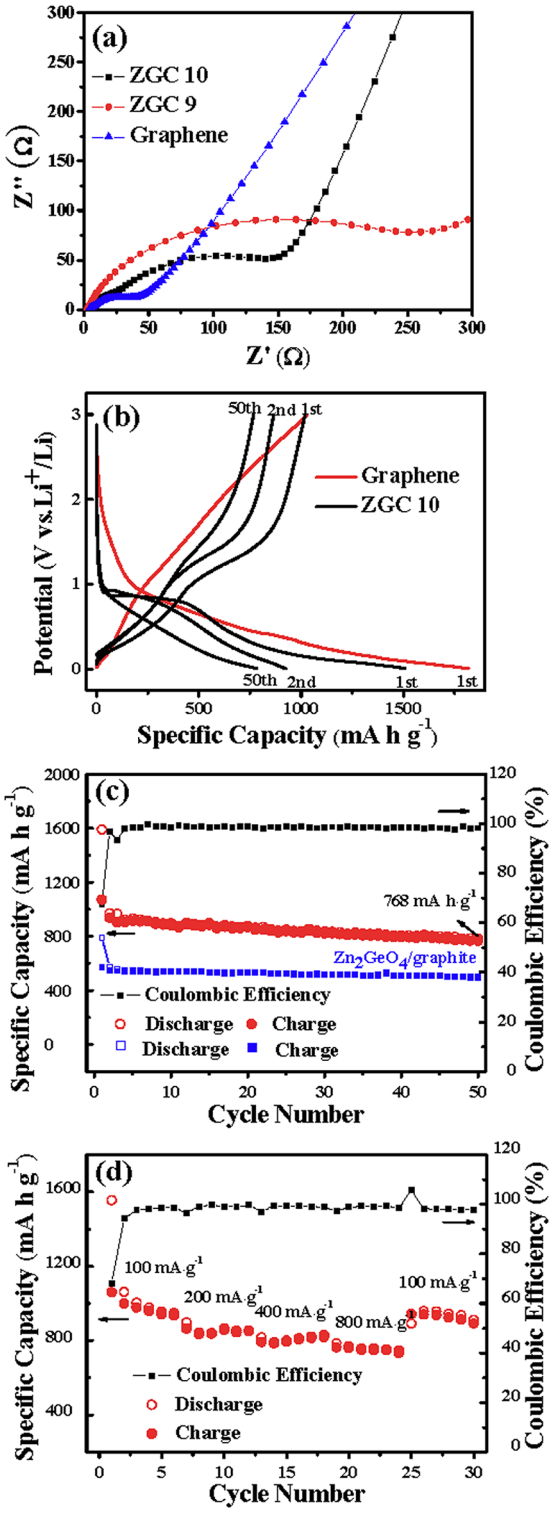

Figure 2. (a) Electrochemical impedance spectroscopy (EIS) plots of graphene, ZGC9, and ZGC10 electrodes after the 1st cycle. (b) Galvanostatic charge−discharge profiles of ZGC10 cycled at 1st, 2nd, and 50th cycles at the current density of 200 mA g^{-1}. (c) Cycling performance and Coulombic efficiency of ZGC10 electrode at the current density of 200 mA g^{-1} for 50 cycles; cycling performance of Zn_2GeO_4 particle/graphite (containing 80 wt % graphite) at 50 mA g^{-1} for 50 cycles was also shown for comparison (blue curve). (d) Rate capability and Coulombic efficiency of the ZGC10 electrode.

composite electrodes, an obvious discharge plateau at ~0.8 V in the 1st discharge curve was observed (Figure S7). Interestingly, the 1st discharge capacity was up to 1508 mA h g^{-1}, and the 1st charge capacity of 1020 mA h g^{-1} was retained, thereby leading to an impressive Coulombic efficiency of 67.6%. We note that the initial capacity loss resulted from the incomplete conversion reaction and the formation of a solid electrolyte interphase (SEI) layer due to the decomposition of electrolyte.[21]

When the 2nd charge/discharge cycling was conducted, the plateau slightly raised to around 0.92 V owing to the decrease in surface energy of ZGC10.[22] The charge capacities of partially crystalline ZGC10 were 867 and 768 mA h g^{-1} at the 2nd and 50th discharge processes, respectively. In contrast, for graphene, no obvious voltage plateau was seen, and the 1st discharge and charge capacities were 1819 and 1029 mA h g^{-1}, respectively. We note that single graphene typically suffers from the stacking of one sheet over another, resulting in multilayer graphene sheets, which lead to serious irreversible capacity despite its high initial discharge capacity (as high as 2042 mA h g^{-1}).[23−25] However, the agglomeration of graphene between layers can be prevented to retain their highly active surface area by anchoring other nanostructures on the single graphene sheet.[13] The discharge/charge cyclabilities of ZGC10 (Figure 2c), ZGC9 (Figure S8b), and graphene electrodes at the current density of 200 mA h g^{-1} for 50 cycles and pure Zn_2GeO_4 electrode for 13 cycles (Figure S8a) were measured. The 1st discharge and charge capacities were 1508 and 1020 mA h g^{-1} for ZGC10, 1585 and 940 mA h g^{-1} for ZGC9, 1819 and 1029 mA h g^{-1} for graphene, and 1375 and 587 mA h g^{-1} for pure Zn_2GeO_4, respectively. Obviously, the discharge and charge capacities of ZGCs measured experimentally were higher than the calculated capacities, that is, an extra discharge capacity of 88 mA h g^{-1} and an extra charge capacity of 388 mA h g^{-1} for ZGC10, respectively (see Supporting Information). This explicitly suggested that the interaction between partially crystalline Zn_2GeO_4 and graphene promoted the lithium storage performance of composites. The extra discharge capacity can be attributed to the decomposition of electrolyte and the larger electrochemical active surface area contributed by graphene.[23,26] The specific capacity of pure Zn_2GeO_4 electrode was reduced to 114 mA h g^{-1} after 13 cycles (Figure S8a). As an intriguing comparison, Zn_2GeO_4 /graphite composites (containing 80 wt % graphite) have the discharge/charge capacities of 496 mA h g^{-1} (50th cycle) (Figure 2c). As the amount of Zn_2GeO_4 particles increased, the discharge/charge capacities of Zn_2GeO_4 /graphite composites were appeared at ~400 mA h g^{-1} (50th cycle) owing to the subtle balance between high theortical capacity of Zn_2GeO_4 and the limited accommodation of the volume expansion for Zn_2GeO_4 from graphite in mechanically mixed Zn_2GeO_4 /graphite composites (Figure S9).

The charge capacity of ZGC10 remained at 768 mA h g^{-1}, representing a 88.6% retention of the 2nd charge capacity after the 50th cycles. The Coulombic efficiency exhibited a rapid rise from 67.6% of the 1st cycle to approximately 100% after the 2nd cycle and beyond. A comparable capacity of 514 mA h g^{-1} was observed after 50 cycles under a large current density of 0.8 A g^{-1}(Figure S8d) for ZGC10, suggesting a Coulombic efficiency of nearly 100%.

To further scrutinize the electrochemical performance, rate capacities of partially crystalline ZGCs were carried out at various current densities between 100 mA g^{-1} and 0.8 A g^{-1} (Figure 2d and Figure S8c). The reversible specific capacity of

dx.doi.org/10.1021/la501830r | Langmuir 2014, 30, 8215−8220

780 mA h g^{-1} for ZGC10 at the current density of 0.8 A g^{-1} indicated a markedly improved rate performance as compared to the previous two reports on highly crystalline pristine Zn_2GeO_4 nanorods under 0.8 A g^{-1}, i.e., ~600 mA h g^{-1} [3] and almost 0, respectively.[6] The above-mentioned reversible specific capacity of ZGC10 is much higher than that (~300 mA h g^{-1}) of Zn_2GeO_4 particle/graphite composites (containing 60 wt % graphite) at 0.2 A g^{-1} (Figure S10). Most importantly, a reversible specific capacity of 892 mA h g^{-1} for ZGC10 was retained when the current density returned to 100 mA g^{-1} after the charge and discharge cyclings at various current densities (Figure 2d). Moreover, the Coulombic efficiency of partially crystalline ZGC10 was also nearly 100% at the different current densities (Figure 2d). This remarkable rate capacity can be reasonably ascribed to the presence of both the amorphous regions in ZGCs and the elastic, highly conductive graphene sheets, which imparted the accommodation of the volume expansion of Zn_2GeO_4 nanorods, ensuring their structural stability even under large current density.

The XRD measurements were carried out to identify the phase compositions of ZGC10 electrode after the 1st discharge to 0.01 V and the 1st charge to 3 V (i.e., curves 1 and 2 in Figure 3a, respectively). In curve 1, the diffraction peaks of Li_2O, Zn, Ge, $Li_{11}Ge_6$, and $Li_{3.5}Zn_{0.5}GeO_4$ were found, and the remaining peaks resulted from the decomposition of the electrolyte. In a stark contrast, the diffraction peaks noted above disappeared and the peaks of ZnO and GeO_2 emerged (curve 2) when the ZGC10 electrode was charged to 3.0 V. The disappearance of Li_2O after the 1st charge suggested that the decomposition reaction of Li_2O was reversible.

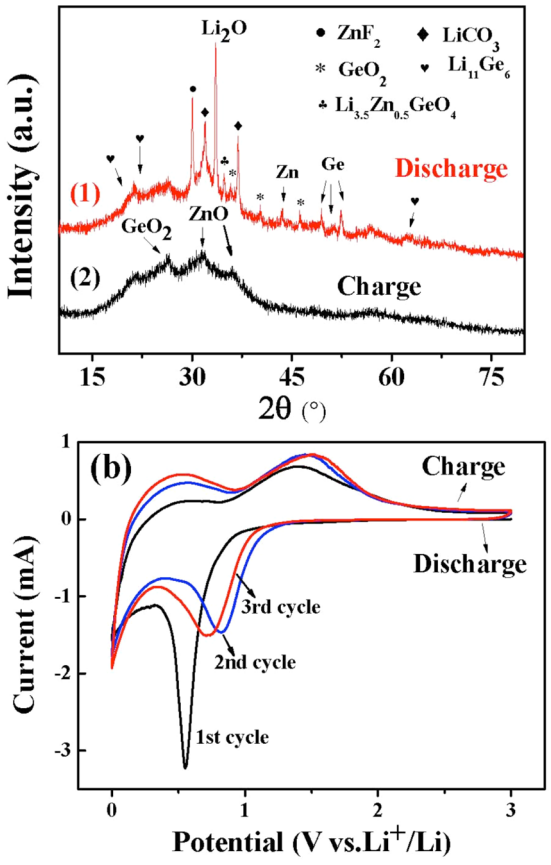

Figure 3. (a) XRD patterns of ZGC10 electrode after the 1st cycle of charge at 3 V and discharge at 0.01 V. (b) Cyclic voltammograms of ZGC10 electrode at 0.5 mV/s scanning rate between 0 and 3.0 V.

To elucidate the electrochemical reaction mechanism of partially crystalline ZGCs, the first three cyclic voltammograms (CV) scans of ZGC10 electrode were performed (Figure 3b). CV scans of Zn_2GeO_4/graphite composite electrodes were also conducted as comparison (Figure S11). The CV curves obtained from ZGC10 were similar to that of purely crystalline Zn_2GeO_4 [3] or Zn_2GeO_4 particle/graphite composites. On the basis of the XRD results and the reaction mechanism of purely crystalline[3] and amorphous[7] Zn_2GeO_4, the mechanism of Li insertion and extraction in ZGCs can be proposed as follows. In the 1st cathodic scan that was carried out from an open circuit voltage of 3.0 V, a sharp peak appeared at about 0.55 V, corresponding to the decomposition of Zn_2GeO_4 (eq 2 in Supporting Information) accompanied by the formation of SEI films and alloying reactions (eqs 4 and 5 in Supporting Information) between Li and Ge (and Zn).[3] During the 1st anodic scan, two obvious peaks at 0.5 and 1.4 V were observed (Figure 3b), which can be assigned to the delithiation of Li−Ge and Li−Zn alloys at 0.5 V (eqs 6 and 7 in Supporting Information), followed by the reoxidation of two metals to form GeO_2 and ZnO at 1.4 V (eqs 8 and 9 in Supporting Information). The reversible formation of Li_2O buffer layer accommodated the volume change during the delithiation and lithiation processes. We note that the CV curves did not show a recognizable difference in the peak shapes between the subsequent two scans and the first one, except a large peak shift to high potentials (i.e., during the discharge process). The almost overlapped peaks after the 2nd scan during the charge process indicated that Li^+ was fully participated in the charge/discharge processes due to the good reversibility of the electrochemical reaction in ZGCs after they were activated.[6,27] The irreversible capacity in the initial cycles may partially be attributed to the multistep reaction of Zn_2GeO_4. The formed amorphous Li_2O reacted reversibly with Zn and Ge during the subsequent cycles and provided a buffer to restrict the volume change.

It is noteworthy that the 1st reversible specific capacity of partially crystalline ZGC10 electrode (1020 mA h g^{-1}; Figure 2c) was larger than those previously reported in purely crystalline Zn_2GeO_4 nanorods (995 mA h g^{-1}),[3] crystalline Zn_2GeO_4 nanorods/N-doped graphene (870 mA h g^{-1}),[6] and amorphous Zn_2GeO_4 (560 mA h g^{-1}).[7] The initial Coulombic efficiency (67.6%; Figure 2d) of partially crystalline ZGC10 electrode was also higher than that of amorphous Zn_2GeO_4 (34%),[7] crystalline Zn_2GeO_4 nanorods (54%),[3] and crystalline Zn_2GeO_4 nanorods/N-doped graphene (59.7%).[6] Specifically, partially crystalline ZGC10 (containing only 10.2 wt % graphene) pocsessed a reversible specific capacity of 768 mAh/g in the 50th cycle at the current density of 200 mA/g and a comparable rate performance (780 mA h g^{-1} at the current density of 0.8A g^{-1}). The latter was slightly higher than that of Zn_2GeO_4 nanorods/N-doped graphene (containing 27.8 wt % graphene; 773 mA h g^{-1} at the current density of 0.8A g^{-1}).[6] In the present study, a facile two-step hydrothermal processing of Zn_2GeO_4 with the addition of a small amount of graphene was employed to synthesize intriguing partially crystalline ZGCs that comprised crystalline and amorphous regions in a single Zn_2GeO_4 nanorod. This strategy may be utilized for the large-scale production of ZGCs at relatively low cost due to the use of less graphene.

dx.doi.org/10.1021/la501830r | Langmuir 2014, 30, 8215−8220

The impressive performance of partially crystalline ZGCs electrodes for LIBs may be rationalized in the following. (i) The amorphous region in partially crystalline Zn_2GeO_4 nanorods was provided as the buffer layer, which would not suffer from stresses due to the phase transition, and thus facilitated the accommodation of the volume change during lithiation and delithiation.[7] (ii) The elastic graphene sheets covering the Zn_2GeO_4 nanorod surface enhanced the conductivity of the resulting ZGC electrode. They served as effective elastic buffer spacers, which may prevent Zn_2GeO_4 nanorods from aggregation, cracking, or crumbling during the Li^+ insertion/extraction processes, thereby imparting the accommodation of the volume change of Zn_2GeO_4 nanorods as well. In comparison, mechanically mixed graphite only exerted a limited influence in high weight ratio (80 wt % graphite). Taken together, the volume change of the crystalline region of partially crystalline Zn_2GeO_4 nanorods can be readily accommodated by the incorporation of elastic, high-conductivity graphene covered on the surface in conjuction with the presence of the amorphous region of Zn_2GeO_4 nanorods. Consequently, the partially crystalline ZGC electrodes yielded the enhanced energy storage capacity, high Coulombic efficiency, and commendable cycling stability.

CONCLUSIONS

In summary, a two-step hydrothermal method was developed to produce Zn_2GeO_4 nanorod/graphene composites (ZGCs) composed of partially crystalline Zn_2GeO_4 nanorods tightly covered and anchored by graphene sheets. The amorphous region of Zn_2GeO_4 nanorods and the elastic graphene sheets rendered the accommodation of the volume change of ZGCs during the charge and discharge processes. An impressive electrochemical performance was found to exist in the ZGC containing 10.2 wt % graphene (i.e., ZGC10), including a high reversible capacity of 1020 mA h g^{-1} at the 1st cycle, a commendable cyclic performance of 768 mA h g^{-1} after 50 cycles, a nearly 100% Coulombic efficiency, and a good rate capability (780 mA h g^{-1} at the current density of 0.8 A g^{-1}), signifying the promising potential of ZGCs as anode materials for high performance LIBs.

ASSOCIATED CONTENT

Supporting Information

Synthesis of Zn_2GeO_4 nanorods and submicron-sized particles; preparation of CR2032-type coin cells; TGA curves of partially crystalline Zn_2GeO_4/graphene composites (ZGCs); SEM image of ZGC10; XPS spectra of partially crystalline ZGC10; Raman spectra of the as-synthesized partially crystalline ZGC 10; TEM images, SAED and FFT patterns of partially crystalline ZGCs; XRD pattern and TEM images of submicron-sized Zn_2GeO_4 particles prepared by the solid-state method; equivalent electrical circuit analysis; galvanostatic charge−discharge profiles of Zn_2GeO_4 particle/graphite composites; cycling performance of the ZGC composite electrodes; cycling performance of the Zn_2GeO_4 particle/graphite composite electrodes; rate capability and Coulombic efficiency of Zn_2GeO_4/graphite composites; calculation of specific capacities of partially crystalline ZGC10; CV scans of Zn_2GeO_4 particle/graphite composites; and Li insertion and extraction mechanism of partially crystalline Zn_2GeO_4. This material is available free of charge via the Internet at http://pubs.acs.org.

AUTHOR INFORMATION

Corresponding Authors

*E-mail chwsp@scut.edu.cn; Fax +86-20- 87112897 (S.W.).
*E-mail zhiqun.lin@mse.gatech.edu; Tel +1 404 385 4404 (Z.L.).

Notes

The authors declare no competing financial interest.

ACKNOWLEDGMENTS

We gratefully acknowledge the financial support from the Chinese Scholarship Council (S.W.) and Georgia Institute of Technology (Z.L.).

REFERENCES

(1) Zhou, G.; Wang, D.; Li, F.; Zhang, L.; Li, N.; Wu, Z.; Wen, L.; Lu, G. Q.; Cheng, H. Graphene-wrapped Fe_3O_4 anode material with improved reversible capacity and cyclic stability for lithium ion batteries. *Chem. Mater.* **2010**, *22* (18), 5306−5313.
(2) Wang, Q.; Wen, Z. H.; Li, J. H. A hybrid supercapacitor fabricated with a carbon nanotube cathode and a TiO_2−B nanowire anode. *Adv. Funct. Mater.* **2006**, *16* (16), 2141−2146.
(3) Feng, J. K.; Lai, M. O.; Lu, L. Zn_2GeO_4 Nanorods synthesized by low-temperature hydrothermal growth for high-capacity anode of lithium battery. *Electrochem. Commun.* **2011**, *13* (3), 287−289.
(4) Hwa, Y.; Park, C.; Yoon, S.; Sohn, H. The effect of Cu addition on Ge-based composite anode for Li-ion batteries. *Electrochim. Acta* **2010**, *55* (9), 3324−3329.
(5) Zhu, X. J.; Geng, L. M.; Zhang, F. Q.; Liu, Y. X.; Cheng, L. B. Synthesis and performance of Zn_2SnO_4 as anode materials for lithium ion batteries by hydrothermal method. *J. Power Sources* **2009**, *189* (1), 828−831.
(6) Zou, F.; Hu, X.; Sun, Y.; Luo, W.; Xia, F.; Qie, L.; Jiang, Y.; Huang, Y. Microwave-induced in situ synthesis of Zn_2GeO_4/N-doped graphene nanocomposites and their lithium-storage properties. *Chem.—Eur. J.* **2013**, *19* (19), 6027−6033.
(7) Yi, R.; Feng, J.; Lv, D.; Gordin, M. L.; Chen, S.; Choi, D.; Wang, D. Amorphous Zn_2GeO_4 nanoparticles as anodes with high reversible capacity and long cycling life for Li-ion batteries. *Nano Energy* **2013**, *2* (4), 498−504.
(8) Chan, C. K.; Peng, H.; Liu, G.; McIlwrath, K.; Zhang, X. F.; Huggins, R. A.; Cui, Y. High-performance lithium battery anodes using silicon nanowires. *Nat. Nanotechnol.* **2008**, *3* (1), 31−35.
(9) Liu, H.; Wang, G.; Park, J.; Wang, J.; Liu, H.; Zhang, C. Electrochemical performance of α-Fe_2O_3 nanorods as anode material for lithium-ion cells. *Electrochim. Acta* **2009**, *54* (6), 1733−1736.
(10) Yang, J.; Winter, M.; Besenhard, J. O. Small particle size multiphase Li-alloy anodes for lithium-ion batteries. *Solid State Ionics* **1996**, *90* (1−4), 281−287.
(11) Wu, S.; Wang, Z.; Ouyang, X.; Lin, Z. Core-shell Zn_2GeO_4 nanorods and their size-dependent photoluminescence properties. *Nanoscale* **2013**, *5* (24), 12335−12341.
(12) Yang, P.; Zhao, D.; Margolese, D. I.; Chmelka, B. F.; Stucky, G. D. Generalized syntheses of large-pore mesoporous metal oxides with semicrystalline frameworks. *Nature* **1998**, *396* (6707), 152−155.
(13) Wu, Z.; Ren, W.; Wen, L.; Gao, L.; Zhao, J.; Chen, Z.; Zhou, G.; Li, F.; Cheng, H. Graphene anchored with Co_3O_4 nanoparticles as anode of lithium ion batteries with enhanced reversible capacity and cyclic performance. *ACS Nano* **2010**, *4* (6), 3187−3194.
(14) Stoller, M. D.; Park, S.; Zhu, Y.; An, J.; Ruoff, R. S. Graphene-based ultracapacitors. *Nano Lett.* **2008**, *8* (10), 3498−3502.
(15) Novoselov, K. S.; Geim, A. K.; Morozov, S. V.; Jiang, D.; Zhang, Y.; Dubonos, S. V.; Grigorieva, I. V.; Firsov, A. A. Electric field effect in atomically thin carbon films. *Science* **2004**, *306* (5696), 666−669.
(16) Lian, P.; Zhu, X.; Liang, S.; Li, Z.; Yang, W.; Wang, H. Large reversible capacity of high quality graphene sheets as an anode material for lithium-ion batteries. *Electrochim. Acta* **2010**, *55* (12), 3909−3914.

(17) Hummers, W. S.; Offeman, R. E. Preparation of graphitic oxide. *J. Am. Chem. Soc.* **1958**, *80* (6), 1339−1339.
(18) Song, W.; Xie, J.; Hu, W.; Liu, S.; Cao, G.; Zhu, T.; Zhao, X. Facile synthesis of layered Zn_2SnO_4/graphene nanohybrid by a one-pot route and its application as high-performance anode for Li-ion batteries. *J. Power Sources* **2013**, *229* (0), 6−11.
(19) Si, Y.; Samulski, E. T. Exfoliated graphene separated by platinum nanoparticles. *Chem. Mater.* **2008**, *20* (21), 6792−6797.
(20) Reddy, M. V.; Subba Rao, G. V.; Chowdari, B. V. R. Nano-$(V_{1/2}Sb_{1/2}Sn)O_4$: a high capacity, high rate anode material for Li-ion batteries. *J. Mater. Chem.* **2011**, *21* (27), 10003−10011.
(21) Yao, W.; Yang, J.; Wang, J.; Nuli, Y. Multilayered cobalt oxide platelets for negative electrode material of a lithium-ion battery. *J. Electrochem. Soc.* **2008**, *155* (12), A903.
(22) Liu, H.; Bo, S.; Cui, W.; Li, F.; Wang, C.; Xia, Y. Nano-sized cobalt oxide/mesoporous carbon sphere composites as negative electrode material for lithium-ion batteries. *Electrochim. Acta* **2008**, *53* (22), 6497−6503.
(23) Yoo, E. J.; Kim, J.; Hosono, E.; Zhou, H. S.; Kudo, T.; Honma, I. Large reversible Li storage of graphene nanosheet families for use in rechargeable lithium ion batteries. *Nano Lett.* **2008**, *8* (8), 2277−2282.
(24) Pan, D.; Wang, S.; Zhao, B.; Wu, M.; Zhang, H.; Wang, Y.; Jiao, Z. Li storage properties of disordered graphene nanosheets. *Chem. Mater.* **2009**, *21* (14), 3136−3142.
(25) Tung, V. C.; Allen, M. J.; Yang, Y.; Kaner, R. B. High-throughput solution processing of large-scale graphene. *Nat. Nanotechnol.* **2009**, *4* (1), 25−29.
(26) Peña, J. S.; Sandu, I.; Joubert, O.; Pascual, F. S.; Areán, C. O.; Brousse, T. Electrochemical reaction between lithium and β-quartz GeO_2. *Electrochem. Solid-State Lett.* **2004**, *7* (9), A278−A281.
(27) Han, F.; Li, W.-C.; Lei, C.; He, B.; Oshida, K.; Lu, A.-H. Selective formation of carbon-coated, metastable amorphous $ZnSnO_3$ nanocubes containing mesopores for use as high-capacity lithium-ion battery. *Small* **2014**, DOI: 10.1002/smll.201400371.